Evaluation of Normal Tissue Complication Probability and Risk of Second Primary Cancer in Prostate Radiotherapy

Rungdham Takam

Thesis submitted for the degree of
Doctor of Philosophy
in
The School of Chemistry and Physics,
The University of Adelaide

Supervisors
A/Prof. Eva Bezak
Prof. Eric E. Yeoh
Dr. Guilin Liu

April 2010

Chapter 7

Peripheral photon and neutron doses from prostate cancer external beam irradiation and the risk of second primary cancers

7.1 Introduction

In Chapter 6, the radiation dosimetry technique based on ^{6}LiF:Mg,Cu,P and ^{7}LiF:Mg,Cu,P glass-rod TLDs was proposed to measure the ambient out-of-field photons and neutrons produced during the irradiation using 18 MV beam from Varian iX medical linear accelerator. Exposure to these radiations is associated with some (possibly small) risk of developing radiation-induced carcinogenesis in the organs/tissues distal to the target volume.

In the report of Xu *et al* (2008), the patient's anatomy was divided into three regions for treatment planning purposes: (i) directly irradiated target (tumour) area characterized by the Gross Tumour Volume (GTV), Clinical Target Volume (CTV), and Planning Target Volume (PTV) which may include partial volumes of organs-at-risk; (ii) the organs-at-risk which are located next to the tumour and do not intersect directly with the beam path and are allowed to receive intermediate-level (5 – 50 Gy) radiation doses; and (iii) the rest of the patient's body which is typically not covered by any therapeutic or diagnostic imaging procedure and may receive low-level (<5 Gy) scattered doses from the accelerator head and radiation scattered within patient's body. Estimation of the Second Primary Cancer (SPC) risks as described in Chapter 5 involves the OARs situated in the first and second regions according to Xu *et al* description. Dose distributions within the volumes of normal tissues located in this region can be obtained from dose-volume histograms which are usually available for risk analysis. However, the organs located in the third region such as lungs, heart, thyroid, and organs in gastrointestinal tracts are not normally contoured during the treatment planning process. Therefore, the dose-volume histograms of these organs are generally not available for risk estimation. In fact, current modern radiation treatment planning systems do not calculate doses from secondary radiations and the dose calculation for distal organs can be quite unreliable. This hinders the use of archived planning system-derived dosimetric data for relating distal organ doses to SPC risk. As a result, the distributions of doses in these organs must be measured directly.

Prior to 1970s, attention on scattered radiations and their potential to induce second cancers in patients was limited but later on especially during the 1970s and 1980s a number of experimental and theoretical investigations on secondary photon and neutron exposures of patients as well as environment from widely used radiation therapy techniques were performed. As a result, understanding of dose distributions inside patients who underwent radiation treatments has been greatly improved. A comprehensive report regarding measurements of secondary radiations with respect to induction of second cancers is provided in the publication of Xu *et al* (2008). A summary of published reports regarding the peripheral dose measurements and risk of second malignancy are shown in Table 7.1 and some of these reports are discussed in the following sections.

Table 7.1. *Summary of several reports on the measurements of peripheral neutron doses produced from medical linear accelerators and risk of second primary cancer.*

References	Method	Machine/ Treatment	Results
Liu *et al* (1997)	EGS4-MORSE Monte Carlo simulation	Varian Clinac 2100C/2300C	Neutron ambient dose equivalent (H_n) at 1 meter from isocentre on the patient plane: 1) 20 MV: 1.78 mSv/Gy 2) 18 MV: 1.50 mSv/Gy 3) 15 MV: 0.72 mSv/Gy 4) 10 MV: 0.02 mSv/Gy
D'Errico & Nath (1998)	1. Passive, integrating superheated bubble detector in tissue-equivalent phantom (Plexiglas tank) 2. CR-39 NTD for entrance dose at isocentre	18 MV CGR-MeV Saturne 20, 10 x 10 cm^2 field size	*Neutron dose equivalent in Plexiglas phantom* H_n per unit photon dose (mSv/Gy) Depth (cm) / On-axis / 10 cm off-axis / 20 cm off-axis 1 / 4.50 / 2.05 / 1.75 5 / 2.50 / 0.80 / 0.60 10 / 1.50 / 0.30 / 0.20 15 / 1.00 / 0.25 / 0.15 Within primary beam, fast neutrons contributed significantly to total equivalent dose.

Table 7.1. *Continued.*

References	Method	Machine/ Treatment	Results
Ongaro *et al* (2000)	1. MCNP4B-GN Monte Carlo simulation 2. BDS passive bubble spectrometer	ELEKTA SL20I 18 MV and Mevatron Siemens 15 MV	The neutron dose equivalent lies between 1 – 4.8 mSv/Gy depending on accelerator characteristics and distance from isocentre. At 20 cm from isocentre; 1) Siemens Mevatron: ~0.9 mSv/Gy 2) ELEKTA SL20I: ~2.2 mSv/Gy BDS passive bubble spectrometer is insensitive to photons.
Lin *et al* (2001)	1. BF_3 proportional counter in PE sphere (mean E_n) 2. Powdered P_2O_2 for fast & thermal neutron fluences in x-ray field 3. BD-PND bubble detectors for H_n	15 MV Siemens Primus for IMRT	Neutron dose equivalent at isocentre 1) 15 MV & 0 x 0 cm^2 field: 0.17 ± 0.06 mSv/Gy 2) 15 MV & 40 x 40 cm^2 field: 1.84 ± 0.09 mSv/Gy
Barquero *et al* (2002)	1. LiF:Mg, Ti TLDs, TLD-600 for photons and neutrons, and TLD-700 for photons 2. ^{6}LiI(Eu) rem meter for neutron cross-reference	18 MV Siemens KD-S with 40 x 40 cm^2 collimator	*Neutron dose equivalent per treatment Gy measured inside the vault room* Plane & position: Patient AP; Distance from isocentre (cm): 25 – 80; Dose (mSv/Gy): 0.34 – 0.86 Plane & position: Electron gun PA; Distance from isocentre (cm): 82 – 160; Dose (mSv/Gy): 0.36 – 0.69
Chibani & Ma (2003)	MXCNPX Monte Carlo simulation in tissue equivalent phantom	18 MV Siemens Promus and 15 & 18 MV Varian 2160C	*Dose equivalent ratio (mSv/Gy) for various radiations* Beam: 18 MV Siemens; Neutrons: 5.03; Total: 6.63 Beam: 15 MV Varian; Neutrons: 13.3; Total: 15.2 Beam: 18 MV Varian; Neutrons: 20.4; Total: 28.6 Neutron dose equivalent per 1 Gy target dose of 6.05 mSv/ at 50 cm off-axis distance Gy for an 18 MV Varian linac observed.
Waller *et al* (2003)	1. Analytical calculations (Kersey, French, McCall) 2. MCNP-GN Monte Carlo simulation 3. Bubble detector measurements	Varian Clinac 2100, 2300 CD, 21 EX	Neutron dose equivalent At the closest measuring point to the isocentre (157 cm); 1) Semi-analytical: 0.69 mSv/Gy 2) MCNP-GN: 0.542 mSv/Gy 3) Measurements: 0.593 mSv/Gy The dose is the highest in the patient plane, extending laterally outwards from the isocentre.
Vanhavere *et al* (2004)	Free-in-air, 10 cm Plexi-phantom, and Rando phantom' gamma and neutron doses measurements 1. LiF:Mg,Ti TLDs for gamma 2. Bubble detectors for neutron	6 & 18 MV 3D-CRT and IMRT using Varian Clinac 2100 CD	1. No neutron dose for 6 MV beams 2. Free-in-air gamma dose rates are more localized around the isocentre whilst at about 30 – 40 cm from the isocentre neutron dose rates are higher than gamma dose rates. 3. Organ equivalent doses per 2 Gy target dose range from 0.7 mSv (spinal cord) to 10 mSv (colon) for IMRT. 4. For 70 Gy prostate treatment using 18 MV IMRT, effective dose of 1 Sv was estimated and associated to 5% lifetime risk of fatal cancer.

***Table 7.1**. Continued.*

<table>
<tr><th>References</th><th>Method</th><th>Machine/ Treatment</th><th>Results</th></tr>
<tr><td>Zanini et al (2004)</td><td>Monte Carlo (MCNP4B-GN) simulation</td><td>18 MV Varian Clinac 2300 CD</td><td><u>Neutron ambient dose equivalent</u>
1) Jaws 10 x 10 cm^2, MLC 40 x 40 cm^2: 1.7 mSv/MU (15 cm from isocentre)
2) Jaws 40 x 40 cm^2, MLC 10 x 10 cm^2: 2.7 mSv/MU (15 cm from isocentre)
3) Jaws 10 x 10 cm^2, MLC Clinical Configurations: 1.1 mSv/MU (15 cm from isocentre)</td></tr>
<tr><td>Carinou et al (2005)</td><td>1. Monte Carlo N-particle transport code (ver. 4C2) simulation
2. Gold-foil activation for doses validation</td><td>Philips/Elekta SL-18 for 14 MeV electron beam</td><td>1. Ambient neutron dose equivalent at the isocentre was 1.6 mSv/Gy and decreased to 0.6, 0.4, and 0.3 mSv/Gy at 20, 50, and 90 cm from isocentre, respectively.
2. Neutron absorbed dose in a PMMA phantom decreased with depth from 0.1 mGy/Gy at depth of 0.2 cm to 0.02 mGy/Gy at depth of 14.5 cm.</td></tr>
<tr><td>Facure et al (2005)</td><td>Monte Carlo N-particle transport code (ver. 4B) simulation</td><td>Linac with 10 – 25 MeV photon energies</td><td>1. Average neutron energies produced from 15, 18, 20, and 25 MeV photon beams were 1.15, 1.25, 1.31, and 1.46 MeV respectively.
2. The most probable neutron energy produced was 0.5 MeV.</td></tr>
<tr><td>Huang et al (2005)</td><td>Monte Carlo code FLUKA calculations</td><td>9, 10, 15, 18, and 20 MeV electron beams interacted with 4 mm tungsten target</td><td>Photoneutron dose equivalents per 1 Gy X-ray dose at the isocentre were 0.006, 0.016, 0.147, 0.231, and 0.261 mSv for 9, 10, 15, 18, and 20 MeV electron beams, respectively.</td></tr>
<tr><td>Kry et al (2005)</td><td>1. TLD-700 for photons in RT with >10 MV beams
2. TLD-100 for photons in RT with <6 MV beams
3. Moderated gold foils for neutrons with E_n > 0.5 eV
4. Bare gold foils for thermal neutrons</td><td>1. Varian 2100 for 3D-CRT & 18 MV step-and-shoot IMRT
2. Siemens Primus for 6 MV & 15 MV step-and-shoot IMRT</td><td>Neutron dose equivalent (mSv/Gy) in some organs
<table><tr><th rowspan="2">Organ</th><th>3D-CRT</th><th colspan="3">IMRT</th></tr><tr><th>18 MV Varian</th><th>15 MV Varian</th><th>15 MV Siemens</th><th>18 MV Varian</th></tr><tr><td>Colon</td><td>0.98</td><td>0.46</td><td>0.25</td><td>1.20</td></tr><tr><td>Lung centre</td><td>0.71</td><td>0.32</td><td>0.18</td><td>0.87</td></tr><tr><td>Thyroid</td><td>1.04</td><td>0.52</td><td>0.29</td><td>1.27</td></tr><tr><td>Bone marrow</td><td>1.68</td><td>0.90</td><td>0.47</td><td>1.86</td></tr></table>The 18-MV conventional treatment involved both relatively large photon and neutron dose equivalents, with photons predominating near the treatment field and neutrons predominating farther away.</td></tr>
<tr><td>Chen et al (2006)</td><td>1. Monte Carlo code FLUKA calculations
2. He-3 proportional counters
3. Bubble detectors</td><td>10 MV X-ray beam using Varian Clinac 21EX</td><td>1. Neutron fluences were the highest (up to 3.8 x 10^3 cm^{-2} MU^{-1}) with 10 x 10 cm^2 field-size configuration.
2. Different neutron doses were observed at different locations inside treatment room and in the maze.</td></tr>
<tr><td>Harrison et al (2006)</td><td>Peripheral dose measurements in Rando phantom
1. LiF:Mg,Ti (TLD-100) for photon doses
2. Neutron doses estimated from reported data.</td><td>15 MV Siemens Primus H1 for 74 Gy IGRT (two phases, 64 Gy + 10 Gy with smaller PTV)</td><td>1. Neutron doses decrease slowly with distance from isocentre (approx. 0.57 mSv/Gy at isocentre to 0.38 mSv/Gy at 100 cm) whilst photon doses decrease exponentially with distance.
2. Photons contributed larger doses to most of the organs especially those located in vicinity of treated volume.
3. Doses from CT scanning and portal imaging contributed to around 5 – 10% of the total organ dose.</td></tr>
</table>

***Table 7.1**. Continued.*

References	Method	Machine/ Treatment	Results
Howell *et al* (2006)	1. ^{197}Au-based Bonner sphere system for neutrons 2. Harshaw TLD-100 for X-rays 3. DVH analysis	Varian Trilogy for 6 MV & 18 MV beams and Varian 23EX for 15 MV beam	1. Average neutron energies produced for 18 MV conventional 3D-CRT and IMRT were 0.48 MeV and 0.53 MeV. 2. Neutron dose equivalents per 1 Gy target dose in various organs for 18 MV conventional 3D-CRT range from 50 μSv (oesophagus) to 3.1 mSv (gonads).
Becker *et al* (2008)	Neutron doses in EasyCube solid water phantom measured with a paired magnesium and boron coated ionization chambers (IC 30)	15 MV Siemens Primus for 72 Gy crossed 4-field 3D-CRT and 76 Gy 5-field IMRT	1. The neutron doses absorbed to femoral head from 3D-CRT and IMRT for prostate cancer were approximately 30 mSv and 33 mSv respectively. 2. More monitor units used in IMRT were responsible for higher doses to OAR in IMRT.
Jaradat & Biggs (2008)	1. Bubble detector (BD-PND) 2. CR-39 detector (Luxel+)	1. Siemens Mevatron at 9, 12, 15, 18 MeV for intraoperative radiation therapy (IORT) 2. Varian Clinac 2100CD, 21EX, iX at 10, 15, 18 MV for conventional RT	*Neutron yields determined from bubble detector* Conventional linac: Energy (MeV) / Neutron yields (mSv/Gy); Electron-only linac: Energy (MeV) / Neutron yields (mSv/Gy) 9 / 3.9E-3 ± 2.2E-4 — 9 / 1.5E-3 ± 3.0E-4 12 / 2.1E-2 ± 1.0E-2 — 12 / 7.7E-3 ± 3.2E-3 16 / 1.3E-1 ± 5.3E-2 — 15 / 3.0E-2 ± 1.8E-2 20 / 4.2E-1 ± 3.2E-1 — 18 / 1.0E-1 ± 8.1E-2 Leakage from the IORT machine is about a factor of 10 lower than for the conventional machine.
Ruben *et al* (2008)	DVH analysis for organs within planning CT scan volume and TLD-100 dosimetry in Rando phantom for the rest of the body	18 MV 3D-CRT and 6 MV IMRT. Machine used not specified.	No dosimetric data was reported. Following radiotherapy for prostate cancer: 1. Assuming saturation in carcinogenic risk after 4 Gy fractionated dose – IMRT and 3D-CRT were associated with 0.8% and 1.0% risk respectively, and 2. Assuming reduction in carcinogenic risk after 4 Gy fractionated dose – IMRT and 3D-CRT were associated with 0.6% and 0.8% risk respectively.
Wang & Xu (2008)	MOSFET dosimeters in Rando phantom for photons	Varian Clinac 21EX for 6 MV 7-field IMRT and 18 MV 6- & 4-field 3D-CRT	The maximum organ dose equivalents per 1 Gy target dose were 88 mSv (bladder), 96 mSv (testes), and 470 mSv (bladder) for 4-field 3D-CRT, 6-field 3D-CRT, and 7-field IMRT, respectively. Note: MOSFET dosimeter does not measure neutron dose.
Mesbachi (2009)	1. Monte Carlo calculations using MCNPX (ver. 2.4.0) 2. Scanditronix automatic water phantom & an ionization chamber for percentage depth dose profile	18 MV beams using Elekta SL25	1. At 100 cm from the target and with unflattened beam neutron fluences changed by 7% with field size from 10 x 10 cm^2 to 30 x 30 cm^2. 2. Neutron fluences were reduced with using of flattening filter.

Vanhavere *et al* (2004) reported the measured results of free-in-air (ambient) and in the Rando-Alderson phantom for photons and neutrons produced from 6 MV and 18 MV Varian Clinac 2100 CD accelerator for the prostate cancer treatment. In this study, the measurements were carried out using LiF:Mg,Ti (TLD-700) TLDs for photons doses and BD-PND™ and BDT™ bubble detectors for fast and thermal neutron doses, respectively. Two different detectors were used to separate the radiation doses from photons and neutrons. Two different types of neutron detectors were also employed to differentiate the doses from fast and thermal neutrons. Measurement of photon doses in the Rando phantom was performed using the TLD-700 detectors whilst neutron doses had to be measured in the 10 centimeters thick plexi-slab phantoms because the bubble detectors were too large to be placed inside the Rando phantom. The results of this study are shown in Table 7.1. This problem can be resolved if smaller size glass-rod ^{6}LiF:Mg,Cu,P TLDs as demonstrated in Chapter 6 are used to measure the neutron doses. The glass-rod TLDs can be directly placed inside the Rando phantom at various positions to measure radiation doses from photons as well as slow and fast neutrons simultaneously.

In the studies of Kry *et al* (2005), TLD-700 dosimeters were also used to measure the secondary photon doses in the Rando phantom from various prostate treatment techniques. Measured neutron dose equivalents per MU in some organs were shown in Table 7.1. Neutron equivalent doses were determined from neutron fluences measured with the gold foil activation technique. Similar to the previous study of Vanhavere *et al* (2004), determinations of the organ doses due to photon exposure were done directly

from the readings of TLD-700 dosimeters as these detectors can be directly placed inside the Rando phantom at the locations corresponding to the organs-of-interest. Determination of the organ neutron doses was performed through several steps of measurements and calculations. The final dose equivalents from 12 neutron fluence components at each distance from the central axis were propagated to tissue depth based on the depth of each measurement point and the neutron depth dose equivalent curves.

Similar measurements with the Rando phantom were carried out in the study of Harrison *et al* (2006). The organ photon doses from prostate radiotherapy with the Siemens Primus H1 linear accelerator operating at 15 MV were measured with TLD-100 chips. According to the anatomy texts, the positions of organs and tissues of interest were located and several chips were placed at the selected positions to measure organ doses. However, measurements of individual organ doses due to neutrons were not performed. The data from previously reported measurements of neutron fluence was used instead. The summary of findings from this study is shown in Table 7.1. An important suggestion made in this study is that for regions in or near the target volume, TLD measurement is likely to be less accurate than a calculation using a well-developed algorithm used in the current treatment planning systems in combination with accurate ionization chamber measurements of dose distributions in water. Therefore, for organs close to the target volume, use of the treatment planning system (DVHs) is probably the best method for organ dose calculation. In addition, it was also suggested that planning systems are not designed for calculation of doses to distant organs and do not, in any case, include neutron dose estimates. From

these suggestions, it is necessary to perform direct measurements of peripheral organ doses to evaluate the contributions of both photon and neutron doses to the risk of induction of second primary cancers in various distant organs.

Ruben *et al* (2008) compared the intensity-modulated radiotherapy (IMRT) with the three-dimensional conformal radiotherapy (3D-CRT) in terms of carcinogenesis risk for actual clinical scenarios using DVH analysis for normal tissues located within the planning CT scan volume and thermoluminescent dosimetry in the Rando phantom for the rest of the body. The TLDs used in this study was TLD-100 sensitive only to photons. Data for effective neutron dose was obtained from the reports of d'Errico *et al* (2001) and Vanhavere *et al* (2004). The neutron doses at 40 centimeters from the central axis and at 5 centimeters depth were used to represent the dose to distant organs whilst the doses at 7.5 centimeters from the central axis and at 5 centimeters depth were used for tissues within the planning CT volume. Risk estimates associated with these two techniques are summarized in Table 7.1. Although neutron contribution to the total organ doses was not directly measured in this study, it was still necessary to take it into account for second malignancy risk estimations. It is important though to develop a dosimetry technique which can be used to measure photon and neutron doses in the Rando phantom simultaneously. A novel dosimetry technique based on ^{6}LiF:Mg,Cu,P and ^{7}LiF:Mg,Cu,P TLDs has been proposed in the previous chapter and the use of this technique in measurement of peripheral organ doses will be demonstrated in this chapter.

In addition to direct measurement of peripheral radiation doses using various dosimeters as described above, it is also possible to calculate the radiation doses especially from neutrons using Monte Carlo simulation codes such as MCNP (Ongaro *et al* 2000, Chibani & Ma 2003, Waller *et al* 2003, Zanini *et al* 2004, Carinou *et al* 2005, Facure *et al* 2005, Becker *et al* 2007, and Mesbahi 2009) and FLUKA (Huang *et al* 2005 and Chen *et al* 2006). Results from these studies are summarized in Table 7.1. The results obtained with Monte Carlo can be highly detailed and exceptionally accurate depending on the accuracy of the input data and parameters. However, in some cases, especially when modification of the code is required, an experienced operator is needed to perform the simulation. In addition, a long simulation time may be required especially for low threshold (cut-off) energies. Furthermore, results of the simulation need to be verified against the results from actual measurement.

It is clear that photon doses inside the Rando phantom can be easily measured using small size detectors like either TLD-100 or TLD-700. TLD-700 dosimeter is sensitive exclusively to photons whilst TLD-100 containing small traces of lithium-6 isotope is sensitive to photons and to a lesser extent also to neutrons.

Measuring neutron doses inside the Rando phantom appears to be more difficult considering that most of the neutron dosimeters are of large sizes and cannot be fitted into the Rando phantom slices for direct dosimetry. In addition, the neutron dosimeters such as bubble detector, nuclear track film, and gold foil activation technique require special reading process and equipment which may not be generally available in a regular radiotherapy facility. While the neutron survey meter such as AN/PDR-70 may also be used for neutron dosimetry due

to its ability to measure neutrons over very wide energy ranges, it is very bulky and cannot be used inside the phantom (ICRU, 1969). In contrast, TLDs are commonly used in many radiotherapy laboratories because of their easy-to-handle and operate properties. Another significant characteristic of the TLDs is that they do not suffer from pile-up and dead-time effects like the active dosimeters (Barquero *et al* 2002). Therefore, for the purpose of measuring peripheral photon and neutron doses in the Rando phantom, the LiF:Mg,Cu,P either enriched with Li-6 and Li-7 glass-rod TLDs are used in this thesis.

It has been demonstrated in the previous chapter that the radiation dosimetry technique based on ^{6}LiF:Mg,Cu,P and ^{7}LiF:Mg,Cu,P glass-rod TLDs can be used to evaluate the radiation doses from photons and neutrons produced by high-energy linear accelerator. In this chapter, the peripheral photon and neutron doses resulting from prostate carcinoma EBRT in the anthropomorphic Rando phantom were determined from the TLD readouts. The risk of developing SPCs was then estimated using the linear term only and both the linear and quadratic terms of the competitive risk model.

7.2 Materials and methods

7.2.1 Anthropomorphic Rando phantom

The anthropomorphic Rando phantom (The Phantom Laboratory, NY) as shown in Figure 7.1 is made of radiologically soft tissue equivalent material (synthetic isocyanate rubber) and is also constructed with a natural human skeleton inside the material. The density of the soft tissue equivalent material is 0.985 g/cm^3 with an effective atomic number of 7.30 (Lanzl 1995). In this phantom, the

lower-density material is also used to construct the natural human lungs which are molded to fit the contours of the rib cage. The exact density of material representing lungs is not specified but it is claimed to have the same effective atomic number as the soft tissue material with a density which simulates lungs in a median respiratory state. The Rando phantom consists of 35 slices with a thickness of 2.5 centimeters per slice except the lowest (35^{th}) slice which has thickness of 6.5 centimeters. In each slide, a number of grid holes are drilled through the phantom's soft tissue material. The close-fitting Mix D plugs inserted in the holes can be removed to insert the radiation dosimeters which, in this thesis, are ^{6}LiF:Mg,Cu,P and ^{7}LiF:Mg,Cu,P glass-rod TLDs.

Figure 7.1. (Left) *The anthropomorphic Rando phantom consisting of 35 section slices. The phantom sections are individually numbered and all sections are assembled in the clamping device.* ***(Right)*** *A section of the Rando phantom was shown. The area of the lower density material (darker color enclosed by the green line) simulating the human lung tissue is displayed. The grid holes with white Mix D plugs are also shown. The rib cage bones made of true human skeleton can also be seen in this phantom section (yellow circle).*

7.2.2 ^{6}LiF:Mg,Cu,P and ^{7}LiF:Mg,Cu,P glass-rod TLDs

General properties, calibrations and processing of ^{6}LiF:Mg,Cu,P and ^{7}LiF:Mg,Cu,P glass-rod TLDs have been described previously in section 6.2.1 of Chapter 6. In order to place the TLDs inside the phantom grid holes, reusable TLD plugs have been made from tissue equivalent wax used in radiotherapy. A pair of ^{6}LiF:Mg,Cu,P and ^{7}LiF:Mg,Cu,P TLD rods were placed on a piece of wax (2.0 x 2.5 cm^2) and the wax was rolled to make a plug having the same dimension as the Mix D plug (Figure 7.2). Each TLD plug was also numbered using permanent ink marking pen. In total, 25 TLD plugs were made and inserted into the phantom slices. Each TLD plug can be reused several times and should be replaced when it become bristle or broken.

TLD plugs were inserted in the Rando phantom at the designated positions according to the CT scan images of the phantom especially for the measurements of the lung doses. In this thesis, TLD plugs are inserted in the grid holes of Rando phantom sections number 8 – 10, 12 – 21, and 21 – 30 to measure the doses to thyroid, lungs, and some organs of the digestive system such as stomach, liver, and colon, respectively.

Figure 7.2*. A picture shows a TLD plug made from the tissue equivalent wax and a pair of ^{6}LiF:Mg,Cu,P and ^{7}LiF:Mg,Cu,P TLD rods. A permanent ink marking pen is used to mark the number of the TLD plug.*

7.2.3 Rando phantom irradiations

Irradiations of the Rando phantom were performed using the 18 MV X-ray beam from Varian iX linear accelerator located at the Royal Adelaide Hospital. A total photon dose of 80 Gy (presently used total dose for prostate EBRT) was delivered to the pelvis of the TLD-loaded Rando phantom simulating 4-field 3D-CRT technique with the jaws set at 10 x 10 cm^2 and delivery rate of 300 MU/minute (Figure 7.3). Irradiation was performed with gantry rotated at 0^o, 90^o, 180^o, and 270^o.

Prior to the irradiation of the Rando phantom, 3 pairs of selected ^{6}LiF:Mg,Cu,P and ^{7}LiF:Mg,Cu,P TLD rods were irradiated to 2 Gy radiation dose using 6 MV beam to be used as control TLDs and for the calculation of the *k* coefficient (see section 6.3, Chapter 6). Several ^{6}LiF:Mg,Cu,P and ^{7}LiF:Mg,Cu,P TLD rods were also kept non-irradiated for background correction.

***Figure 7.3**. The TLD-loaded Rando phantom is placed on the treatment couch of the Varian iX linear accelerator. The laser beams were used to set up the phantom on the couch using the coordinates marked on the phantom for pelvic irradiation*.

7.3 Determination of doses from TLD readouts

Conversion of ^{6}LiF:Mg,Cu,P and ^{7}LiF:Mg,Cu,P TLDs reading results to photon and neutron dose equivalents were performed as described in Chapter 6. Briefly, the raw readouts from both TLDs obtained with the Harshaw 3500 TLD reader were corrected for the background, TLD individual Sensitivity Correction Factor (SCF) and TLD Batch Correction Factor (BCF). The corrected readout of each individual TLD was multiplied with corresponding photon and neutron readout-to-dose conversion factors derived from calibrations. The photon readout-to-dose conversion factor for ^{7}LiF:Mg,Cu,P TLDs is 44.6 mSv/ μC**.**

For ^{6}LiF:Mg,Cu,P TLDs, results from the free-in-air neutron dose measurements using CR-39 etch-track detectors were used to cross-reference with the corrected readouts of ^{6}LiF:Mg,Cu,P TLDs to derive distance-dependent readout-to-neutron dose conversion factors. In case of Rando phantom measurements, an approximation was made to derive a single readout-to-neutron dose conversion factor for ^{6}LiF:Mg,Cu,P TLDs. All measuring points in the Rando lie within 65 centimeters distance from the isocentre. From 302 measuring points, their mean distance was 38 centimeters from the isocentre. Using linear interpolation technique and readout-to-neutron dose conversion factors for 30 (50.8 mSv/μC) and 50 (175.7 mSv/μC) centimeter distances obtained from previous chapter resulted in a readout-to-neutron dose conversion factor of 100.8 mSv/μC for 38 centimeters distance in the isocentre which will be used in this chapter to convert corrected readout of ^{6}LiF:Mg,Cu,P TLDs to neutron dose equivalent.

7.4 Estimations of second primary cancer risk

Estimations of SPC risk for specific organ/tissues were performed using the competitive risk model (equations 5.4 and 5.5) described previously in Chapter 5. The exact values of cell survival parameters ($(\alpha/\beta)_1$ and $(\alpha/\beta)_2$) for an individual organ are not commonly available especially for $(\alpha/\beta)_1$ which describes the induction of DNA mutation. The influence of cell survival parameter heterogeneity on predicted risk of second malignancy was discussed in Dasu & Toma-Dasu (2005) and suggestions have been made that α/β parameter may have little influence on the risk curve. Therefore, the values of cell survival parameters as described in the above report were used in the current work. The values of α_1, α_2, and α/β ratio for organs-at-risk are 0.05 Gy^{-1}, 0.25 Gy^{-1}, and 5 Gy, respectively. The α/β ratio of 4.5 Gy and α_1 of 0.017 Gy-1 were also recommended for lungs (Dasu *et al* 2005) but the general values were used in this study. Figure 7.4 shows predicted risk of second malignancy as a function of fractionated dose assuming that an organ-at-risk is irradiated to out-of-field radiation doses as a result of tumour target irradiation to a total dose of 80 Gy (40 fractions of 2 Gy/fraction). The curve was plotted using general cell survival parameters as described above and the risk was calculated using equation (5.4). From the curve, it can be seen that the risk increases with increasing dose and reaches the highest risk (~7%) at the dose around 4 Gy. Sterilization of already mutated cells takes effect when the dose is further increased resulting in decrease of the predicted risk. The risk of second malignancy is approximately 0.1% at 25 Gy dose.

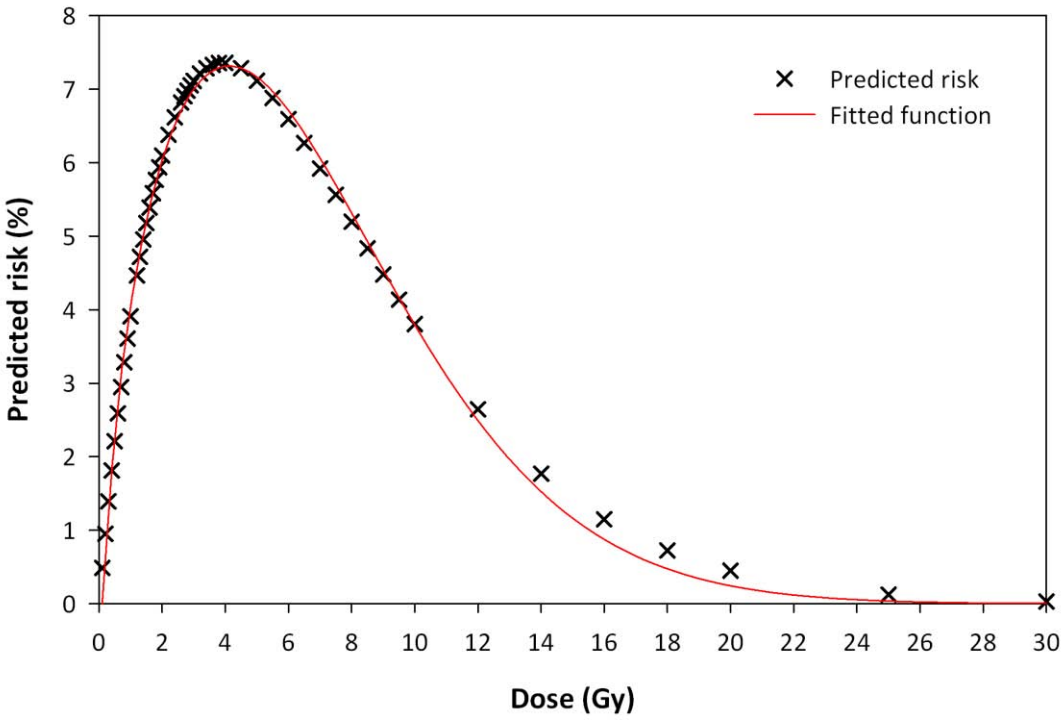

***Figure 7.4**. Predicted risk (%) of radiation-induced second malignancy as a function of fractionated radiation dose.*

The dose data measured in the Rando phantom in combination with the approximated positions of organs in the phantom as described in Harrison *et al* (2006) were applied to determine the photon, neutron, and total dose equivalents delivered to each organ as a result of the prostate irradiation using 4-field standard fractionated 3D-CRT technique with the 18 MV X-ray beam from Varian iX linear accelerator to the total target dose of 80 Gy.

The photon and neutron dose equivalents for each measuring point in every measured slice were calculated. The total dose equivalent for each organ combined of the average photon and neutron dose equivalents which were calculated from measured dosimetric data in individual phantom slices representing that organ. The volumetric dose distribution for the organs-at-risk

(except lungs) was not available thus the average photon and neutron dose equivalents were assumed to be homogeneously distributed over the volumes of the organs-at-risk.

In case of lungs, the dose-volume histogram of lungs (Table 7.4) was reconstructed using differential volume data calculated with Pinnacle^3 treatment planning system (Phillips Medical System, CA) based on the Computed Tomography (CT) images of the lungs in Rando phantom and dosimetric data obtained with TLD measurements. The (differential) second malignancy risk of lung in individual Rando phantom slice was then estimated using the equations (5.4) and the total (integrated) risk of lung SPC was calculated using equation (5.5).

The mean photon, neutron, and total dose equivalents as shown in Table 7.4 were also calculated using the following formalism:

$$Mean\ dose\ equivalent = \overline{H} = \frac{\sum\left(v_i * H_i\right)}{\sum v_i}, \qquad (7.1)$$

where v_i is differential volume (cm^3) which irradiated to dose equivalent H_i (mSv).

Furthermore, standard deviation (S.D) was calculated using following equation:

$$S.D = \sqrt{\frac{\sum\left[v_i\left(H_i - \overline{H}\right)^2\right]}{\sum v_i}}. \qquad (7.2)$$

7.5 Results

7.5.1 Distributions of photon and neutron doses in the Rando phantom

7.5.1.1 Photon doses

Table 7.2 shows the photon dose equivalents (H_{ph}) measured in the Rando phantom as a result of pelvic irradiation to 80 Gy 18 MV photon dose used in this study to simulate the total radiotherapy doses delivered over the course of treatment. The average photon dose equivalent ($\overline{H_{ph}}$) was calculated from dose equivalents measured at different locations in the phantom and from 4 measurements. The variation of the photon dose equivalent as a function of distance from the isocentre is shown in Figure 7.5.

***Table 7.2**. Average peripheral photon dose equivalents ($\overline{H_{ph}}$) in different organs of the Rando phantom as a result of 80 Gy dose irradiation to pelvic using 18 MV 4-field 3D-CRT technique from Varian iX linac measured with the ^{7}LiF:Mg,Cu,P glass-rod TLDs.*

Organs of interest	Rando phantom slices for each organ	$\overline{H_{ph}}$ for 80 Gy dose irradiation in mSv ± S.D (range)	$\overline{H_{ph}}$ per 1 Gy isocentre dose in mSv ± S.D
Thyroid	8 – 10	15.2 ± 3.5 (8.1 – 21.8)	0.2 ± 0.1
Oesophagus	9 – 19	40.4 ± 17.6 (11.8 – 108.0)	0.5 ± 0.2
Liver	19 – 25	133.0 ± 86.3 (21.2 – 512.8)	1.7 ± 1.1
Spleen	20 – 22	96.3 ± 37.5 (28.0 – 203.8)	1.2 ± 0.5

***Table 7.2**. Continued.*

Organs of interest	Rando phantom slices for each organ	$\overline{H_{ph}}$ for 80 Gy dose irradiation in mSv ± S.D (range)	$\overline{H_{ph}}$ per 1 Gy isocentre dose in mSv ± S.D
Stomach	20 – 24	138.4 ± 63.7 (28.0 – 277.3)	1.7 ± 0.8
Kidney	21 – 25	173.7 ± 85.1 (28.0 – 512.8)	2.2 ± 1.1
Pancreas	22 – 23	148.8 ± 35.4 (73.7 – 223.2)	1.9 ± 0.4
Colon (and upper large intestine)	24 – 31	651.2 ± 778.9 (122.0 – 5004.4)	8.1 ± 9.7
Small intestine	24 – 30	521.5 ± 235.5 (122.0 – 2481.4)	6.5 ± 2.9

As expected, the results show that the organs located near the irradiation volume such as small intestine and colon received larger photon dose equivalents than the organs distant from the irradiation volume such as thyroid, oesophagus, and lungs. As the photons scatter from the irradiation volume, they are exponentially attenuated through interactions with the phantom material so the photon dose decreases with increasing distance from the isocentre as shown in Figure 7.4. The distant organs receive X-ray doses partly from X-rays scattered through the body/phantom and also from the leakage photons from the head of the accelerator.

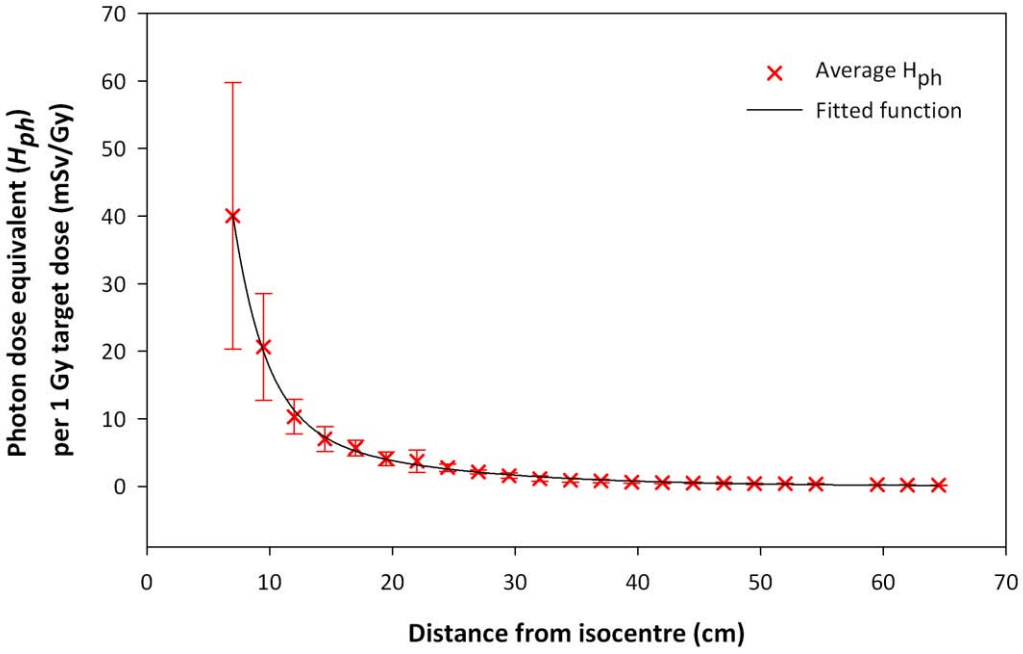

Figure 7.5. *Average peripheral photon dose equivalent per 1 Gy isocentre dose in the Rando phantom measured at different distances from the isocentre. The dose is a result of exposure to external (out-of-field) leakage as well as internal scattered radiations (18 MV X-ray beam from Varian iX linear accelerator).*

7.5.1.2 Neutron doses

Table 7.4 shows the distributions of neutron dose equivalents (H_n) for different organs inside the Rando phantom as a result of pelvic irradiation to 80 Gy using an 18 MV X-ray beam 4-field 3D-CRT technique delivered by Varian iX linac. The neutron dose equivalent (mSv) per 1 Gy isocentre dose as a function of distance from the isocentre is plotted in Figure 7.6. Similarly to photon doses, the neutron dose equivalents near the edge of the irradiation volume are higher than those measured at other positions. However, it can be noticed that at the distance of 30 centimeters and further the average neutron dose equivalents per 1 Gy isocentre dose were relatively constant and larger than that of photons.

***Table 7.3**. Average peripheral neutron dose equivalents ($\overline{H_n}$) in different organs of the Rando phantom as the result of 80 Gy irradiation to pelvic using 18 MV 4-field 3D-CRT technique from Varian iX linac.*

Organs of interest	Phantom slices for each organ/tissue	$\overline{H_n}$ for 80 Gy dose irradiation in mSv ± S.D (range)	$\overline{H_n}$ per 1 Gy isocentre dose in mSv ± S.D (range)
Thyroid	8 – 10	307.8 ± 69.9 (197.5 – 450.2)	3.8 ± 0.9 (2.5 – 5.6)
Oesophagus	9 – 19	451.6 ± 106.7 (197.5 – 709.6)	5.6 ± 1.3 (2.5 – 8.9)
Liver	19 – 25	461.4 ± 135.6 (37.9 – 762.5)	5.8 ± 1.7 (0.5 – 9.5)
Spleen	20 – 22	466.7 ± 123.0 (112.1 – 752.2)	5.8 ± 1.5 (1.4 – 9.4)
Stomach	20 – 24	461.5 ± 135.1 (37.9 – 762.5)	5.8 ± 1.7 (0.5 – 9.5)
Kidney	21 – 25	436.6 ± 145.2 (37.9 – 762.5)	5.5 ± 1.8 (0.5 – 9.5)
Pancreas	22 – 23	465.6 ± 123.1 (264.1 – 762.5)	5.8 ± 1.5 (3.3 – 9.5)
Colon (and upper large intestine)	24 – 31	561.5 ± 429.4 (37.9 – 2098.5)	7.0 ± 5.4 (0.5 – 26.5)
Small intestine	24 – 30	530.7 ± 388.0 (37.9 – 1965.9)	6.6 ± 4.8 (0.5 – 24.6)

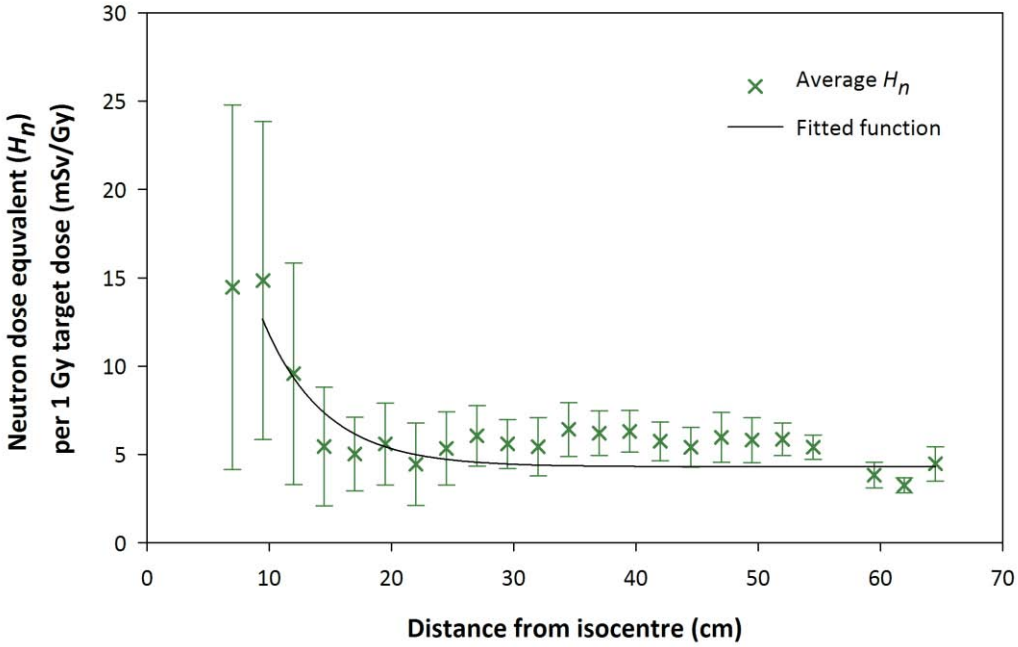

Figure 7.6. *Average peripheral neutron dose equivalent (mSv) per 1 Gy isocentre dose in the Rando phantom as a function of distance (cm) from the isocentre (18 MV X-ray beam from Varian iX linear accelerator).*

7.5.2 Organ doses and risks of second primary cancer

7.5.2.1 Lung dose-volume histogram and risk of second primary cancer

Table 7.4 shows the reconstructed dose-volume histogram of the lungs using differential volumes and dosimetric data obtained with methods described in section 7.4. The competitive risk model (equations 5.4 and 5.5) with cell survival parameters as described earlier (section 7.3) was then applied to the total dose equivalents in the lung dose-volume histogram to calculate the risk of lungs SPC.

Table 7.4*. Dose-volume histogram of lungs reconstructed using differential volume data based on CT images of the Rando phantom and dosimetric data obtained with TLD measurements and associated risk of lungs SPC.*

Phantom slice#	Lungs' volume (v_i) in cm^3	Dose equivalent for 80 Gy dose irradiation in the Rando phantom			Effect (Risk) as a function of Total dose (d_i) *(equation 5.4)*
		Photon dose in mSv	Neutron dose in mSv	Total dose (d_i) in mSv	
12	356.7	26.7 ± 8.3	433.1 ± 54.5	459.8 ± 52.3	0.02
13	395.2	30.0 ± 5.3	468.2 ± 74.0	498.2 ± 72.6	0.02
14	908.0	30.1 ± 8.6	465.1 ± 101.6	495.2 ± 100.9	0.02
15	601.8	37.4 ± 9.7	477.2 ± 112.5	514.6 ± 111.5	0.02
16	747.1	39.2 ± 10.5	432.4 ± 90.9	471.6 ± 91.1	0.02
17	710.9	44.7 ± 10.9	459.8 ± 87.7	504.5 ± 88.8	0.02
18	733.4	50.3 ± 13.9	504.3 ± 94.5	554.6 ± 97.1	0.02
19	349.9	63.1 ± 21.6	496.3 ± 101.3	559.4 ± 98.6	0.02
20	259.6	70.1 ± 24.6	513.3 ± 121.5	583.5 ± 123.6	0.03
21	57.1	91.5 ± 32.3	435.0 ± 132.4	526.5 ± 109.5	0.02
	Total volume = 5119.7 cm^3	Mean = 41.9 ± 12.8 mSv	Mean = 468.9 ± 25.5 mSv	Mean = 510.8 ± 22.0 mSv	(Total) risk of lungs SPC = 2.3 ± 0.5% *(equation 5.5)*

As a result, the estimated risk of lungs SPC obtained with this method was 2.3 ± 0.5%. However, if alternate lung cell survival parameters including α / β ratio of 4.5 Gy and α_1 of 0.017 Gy^{-1} were used, the estimated risk of lungs SPC would be 0.8 ± 0.2%. A lower risk was mostly associated with a lower value of α_1 representing a lower rate of DNA mutation as a function of dose.

7.5.2.2 Organ dose equivalents and risk of second primary cancer

Table 7.5 shows the estimated total dose equivalent (H_{tot}) per 1 Gy isocentre dose and projected total dose equivalent (H_{tot}^{80Gy}) for a full prostate radiation treatment to a total dose of 80 Gy using 4-field standard fractionated (2 Gy/fraction) 3D-CRT technique with the 18 MV beam from Varian iX linear accelerator. The estimated risk of SPC for each organ and corresponding neutron/photon dose equivalent are also shown in this table.

The estimated risk of SPC shown in the Linear column of Table 7.5 is referred to the risk of SPC calculated using the linear term of the competitive risk model which represents the effect of DNA mutations only. In addition, the estimated risk of SPC shown in the Linear-quadratic column of this table is referred to the risk of SPC estimated using the full competitive risk model (both linear and quadratic terms of the equation were used). As described earlier, the photon and neutron dose equivalents were assumed to be uniformly distributed in each organ.

The organs located in the close proximity to the irradiation volume were exposed to relatively larger doses especially from photons compared to the distant organs. In case of the distant organs such as thyroid, and oesophagus they clearly received smaller total doses than organs closer to the irradiation volume, however, the contribution of neutrons to the total dose became larger than that of photons which reflected by a larger neutron/photon dose equivalent ratio.

Table 7.5. *The total organ dose equivalent ($H_{tot}^{80\,Gy}$) and per 1 Gy target dose ($H_{tot}^{1\,Gy}$) corresponding to 80 Gy dose pelvic irradiation using 4-field 3D-CRT technique with 18 MV X-ray beam from Varian iX linear accelerator. The risks of second primary cancer following the full prostate treatment were calculated using the total dose equivalents.*

Organ	$H_{tot}^{1\,Gy}$ in mSv ± S.D (range)	H_{tot}^{80Gy} in mSv ± S.D (range)	Neutron/ Photon dose equivalent ratio	Risk of second primary cancer (% ± S.D) following 80 Gy dose radiotherapy	
				Linear	Linear-quadratic
Thyroid	4.0 ± 0.9 (2.7 – 5.7)	323.0 ± 69.3 (212.9 – 458.3)	20.3	1.6 ± 0.3	1.5 ± 0.3
Oesophagus	6.2 ± 1.4 (2.7 – 9.9)	492.1 ± 112.5 (212.9 – 795.9)	11.2	2.5 ± 0.6	2.2 ± 0.5
Liver	7.4 ± 1.6 (3.4 – 12.3)	594.5 ± 130.4 (268.9 – 985.7)	3.5	3.0 ± 0.7	2.6 ± 0.6
Spleen	7.0 ± 1.5 (3.4 – 10.2)	563.0 ± 117.5 (268.9 – 817.2)	4.8	2.8 ± 0.6	2.5 ± 0.6
Stomach	7.5 ± 1.7 (3.4 – 12.3)	600.0 ± 136.2 (268.9 – 985.7)	3.3	3.0 ± 0.7	2.6 ± 0.7
Kidney	7.6 ± 1.8 (3.4 – 12.3)	610.3 ± 140.9 (268.9 – 985.7)	2.5	3.1 ± 0.7	2.6 ± 0.7
Pancreas	7.7 ± 1.7 (4.5 – 12.3)	614.5 ± 135.7 (356.3 – 985.7)	3.1	3.1 ± 0.7	2.6 ± 0.7
Colon (and upper large intestine)	15.0 ± 13.9 (3.9 – 88.8)	1203.7 ± 1113.7 (315.2 – 7102.9)	0.9	6.1 ± 5.6	4.5 ± 4.2
Small intestine	13.0 ± 9.4 (3.9 – 54.0)	1043.3 ± 753.8 (315.2 – 4320.8)	1.0	5.2 ± 3.8	4.0 ± 3.1

Based on the competitive risk model, the risk of developing SPC in each affected organ increases proportionally with dose as can be seen in the Table 7.5. Colon (and upper large intestine) was irradiated to a larger dose than other organs so its risk of developing SPC (~4.5%) is higher than that for other organs (i.e. 2.6% for pancreas and 1.5% for thyroid). As all organs were irradiated to the radiation dose levels where cells kill started to sterilize already mutated cells, a difference between the risk of SPC calculated with the linear term only and with the linear and quadratic terms of the competitive risk model can be seen especially in the organs located close to treatment target volume, i.e. colon and small intestine.

7.6 Discussion

It was proposed in this thesis that using pairs of ^{6}LiF:Mg,Cu,P and ^{7}LiF:Mg,Cu,P glass-rod TLDs with modified wax holders can be used to measure the peripheral photon and neutron doses in the Rando phantom following the simulated prostate irradiation to 80 Gy dose using 4-field standard fractionated 3D-CRT with 18 MV X-ray beam from Varian iX linear accelerator. Generally, the distributions of photon and neutron observed in this thesis were comparable to the published data (Vanhavere *et al* 2004, Kry *et al* 2005, Wang & Xu 2008). In case of neutron measurement, it was reported that neutron doses measured in phantom for 18 MV linear accelerator range between 0.8 and 2.5 mSv per 1 Gy isocentre dose at a 50 centimeters distance (Vanhavere *et al* 2004). In addition, the organ neutron dose equivalents were found to range between 0.4 – 5.0 mSv/Gy and 0.1 – 3.8 mSv for 18 MV IMRT and 3D-CRT respectively. The neutron dose equivalent per 1 Gy isocentre dose of 6.1 mSv/Gy measured in

tissue equivalent phantom locating at 50 centimeters off-axis distance for 18 MV Varian linear accelerator was also reported by Chibani & Ma (2005). In the current work, the measurements performed using pairs of ^{6}LiF:Mg,Cu,P and ^{7}LiF:Mg,Cu,P TLDs at the same distance and with the same energy of linear accelerator resulted in the average neutron dose equivalent of 6.2 ± 1.3 mSv/Gy (isocentre dose) which was generally higher than the range reported by Vanhavere *et al* (2004) but similar to the value reported by Chibani & Ma (2005). Meanwhile, the average organ neutron dose equivalents were observed to range between 3.8 – 7.0 mSv/Gy which were generally comparable to the reported values. The method used for calibration and determination of the readout-to-neutron dose conversion factor for ^{6}LiF:Mg,Cu,P TLDs may be associated with higher average neutron doses obtained in this study (calibrations of these TLDs and results have been previously discussed in Chapter 6), especially a large conversion factor (100.8 mSv/μC) was used for neutron dose conversion from TLD readout. Despite the use of a single readout-to-dose conversion factor for photon and neutron dose conversion throughout the measurements, the results obtained in current work were generally in good agreement with other published data.

It was observed that the photon dose equivalent per isocentre dose decreased exponentially with the distance from the isocentre whilst that of neutron was relatively constant at approximately 5.0 mSv/Gy with the increased distance for up to 50 centimeters from the edge of the irradiation field. As a result of such dose distributions, the organs located in close proximity to the irradiation volume such as colon and small intestines received larger dose from photons

than that from neutrons and only the organs located distally from the irradiation volume (i.e. lungs, oesophagus, and thyroid) received higher neutron dose than photon dose. The amount of the dose delivered to each organ depends on the relative location of that organ to the treatment volume. The further the organ is located from the isocentre, the lower the dose (especially from photons) delivered to that organ.

Using the dose data obtained from the TLD measurements in the Rando phantom together with the competitive risk model and general cell survival parameters, the risk of developing second primary cancer in various organs were estimated. The risks calculated for these distant organs were relatively higher than the organs located in the second region (see section 7.1) where they usually receive very high doses from prostate radiotherapy. Results from DVHs analysis presented in Chapter 5 revealed that rectum and bladder were irradiated to high radiation doses (mean dose in the 40 – 50 Gy range) from 4-field 3D-CRT techniques for prostate cancer using 18 MV X-ray beam from Varian iX linear accelerator. As a result, the estimated risks of second malignancy in these organs were relatively small (less than 0.6% for all organs and techniques). In contrast, the doses delivered to distant organs as the results of pelvic irradiation to 80 Gy radiation dose using the same technique and accelerator were relatively much lower (average of 656 ± 264 mSv) but these doses are associated with higher probability of second malignancy induction. As a result, the distant organs were associated with much higher risks of radiation-induced SPC (1.5 – 4.5%). In addition, contributions of secondary neutron doses produced from high-energy linear accelerator were taken into consideration of

SPC risk estimation which cannot be done with DVH analysis. This current work has emphasized the importance of actual radiation dose measurement to clinical treatment planning evaluation especially in terms of second malignancy risk evaluation.

Base on the competitive risk model, in case of low doses (<2 Gy), the quadratic terms (represent cell kills) in equation (5.4) are negligible and the effect (in terms of radiation-induced carcinogenesis) of radiation exposure can be approximated as being linear with α_1 being slope of the curve. This hypothesis was tested by applying only the first (linear) term of the competitive risk model to the average total dose equivalent which each organ received and the results were compared with applying both linear and quadratic terms of the model to the same doses. The results showed that the SPC risk estimates obtained with linear term only are slightly different from those obtained with linear-quadratic terms particularly in organs located far from the isocentre (thyroid and oesophagus). However, higher SPC risk estimates obtained using linear term only were observed in colon and small intestine as they received larger doses than other organs. Without taking account of sterilization of already mutated cells as a result of exposure to high radiation dose into SPC risk estimation, over-estimated SPC risk can be found.

In this study, CT images of the Rando phantom were taken and uploaded to the Pinnacle^3 treatment planning system which allows contouring of the lungs in the phantom. Volume of the lungs in each slice were calculated and results of TLD measurements were used with the lungs' volume to construct the dose-volume histogram which was applied to the competitive risk model to estimate

the risk of lung SPC. With this approach, it is possible to determine the lung dose and to estimate the radiation-associated risk of second malignancy. In a case that volumetric data of the lungs is not available for generation of the dose-volume histogram, using the average lung dose derived from TLD measurements in the Rando phantom incorporation with the competitive risk model will result in a similar estimated risk, as confirmed in this study.

According to National Council on Radiation Protection and Measurements (NCRP) report 116, colon, lungs, and stomach are found to be the prime sites which show higher relative probabilities of developing radiation-associated second malignancy compared to other organs (Hall 2006). The risk coefficients assigned for these organs, i.e. 0.85%/Sv for colon and lungs and 1.1%/Sv for stomach, are significantly higher than those for the rest of the body. Therefore, it is necessary to monitor the dose delivered to these organs as a result of external beam radiotherapy in order to determine the associated risk of developing second malignancy in these radiation-sensitive organs. The results from this current work showed that the doses delivered to these and other organs as a result of pelvic external beam irradiation caused elevation in the risk of developing SPCs.

Influence of different radiation treatment techniques for prostate cancer other than 4-field 3D-CRT in peripheral organ dose was not investigated in this work. However, it has been reported that the difference in terms of risk of second malignancy was observed between 3D-CRT and Intensity Modulated Radiotherapy (IMRT) where irradiation of a larger volume of normal organs to lower peripheral doses was indicated (Hall & Wuu 2003). However, Kry *et al*

(2007) suggested that the ratio of risk estimates between different treatment modalities may be statistically significant when there is an effective dose equivalent difference of at least 50%. At the time of this study the IMRT technique was not available at our centre thus comparison between these two techniques in terms of peripheral doses and risk of second malignancy was not performed.

In this study, the estimation of radiation-associated risk of SPC in various organs using the competitive risk model were based on the general cell survival parameters described in Dasu & Toma-Dasu (2005) and Dasu *et al* (2005). The values of these parameters have been described earlier in section 7.4. Although the values of the parameters used in this current work may not represent the actual radiosensitivity characteristics of a specific organ which can be derived from a long term clinical investigation, the estimated risks of SPC presented in this thesis are valid for the purpose of demonstrating the effects of exposure to radiation doses in various organs of interest as a result of prostate irradiation.

In the previous chapter, out-of-field radiation doses from photons and fast neutrons were measured using TLDs whilst thermal neutron doses were derived with the use of cadmium filter in the TLD holder. In this chapter, measurements of peripheral organ doses due to photons and neutrons in the Rando phantom were carried out but it was not possible to use the cadmium filter in the modified wax TLD holder. Therefore, the contribution of thermal neutrons to the total neutron doses was unknown. In addition, the neutron dose equivalents measured in the Rando phantom at the same distance were higher (approximately 8.0 mSv/Gy) compared to that measured in-air (around 1.8

mSv/Gy). The same calibration factor was applied to the total neutron reading thus overestimating the dose due to thermal neutrons.

Similar to ambient out-of-field dose measurements, variations in peripheral dose measurements in the Rando phantom may be also associated with various factors such as directional variations of the dose distributions, statistical variations in production of secondary photons and neutrons originated from random interactions in the head of a linear accelerator, uncertainty of the CR-39 etch-track detector (±20%, Reft *et al* 2006) used for cross-calibration as well as energy dependence in ^{6}LiF:Mg,Cu,P (±50% for E_n from thermal to 20 MeV) TLDs.

7.7 Conclusion

It is demonstrated in this chapter that irradiation of the prostate using high-energy photons (>10 MeV) beams from the Varian iX medical linear accelerator causes irradiation of the distant organs to peripheral photon and neutron doses which consequently leads to increased risk of developing radiation-induced second primary cancers. The radiation dosimetry technique based on the ^{6}LiF:Mg,Cu,P and ^{7}LiF:Mg,Cu,P glass-rod TLDs has been proposed for the purpose of determine the peripheral photon and neutron dose equivalents in the Rando phantom. The locations of organs in the Rando phantom can be identified using the published data and the doses can be approximated using the dosimetric data from the TLD measurements. It is possible to use the competitive risk model with general cell survival parameters to estimate the associated risk of developing radiation-induced SPC in the organs-at-risk.

However, selection of cell survival parameters is important and can affect the value of risk estimate as demonstrated with the case of lungs SPC. Derivation of clinical-based cell survival parameters may be required for better accurate risk estimation. In addition, as discussed earlier in Chapter 5, the model used in the thesis does not account for confounding factors such as age, smoking and dietary habits of patients. Furthermore, the competitive risk model cannot predict time of induction and manifestation of the SPC after radiation exposure even though it has been suggested that the relative risk of SPCs for prostate patients treated by radiotherapy increases with time after exposure to treatment (Liauw *et al* 2006 and Abdel-Wahab *et al* 2008).

One major contribution of this current work is that it demonstrated the use of small glass-rod TLDs with modified holders for simultaneously determination of the peripheral photon and neutron doses as the results of high-energy external beam radiotherapy. This type of measurement usually requires two distinctive types of dosimeters to determine the doses from photons and neutrons separately but the method proposed in this study can simplify the dose measuring process. The use of Rando phantom and its CT images in corporation with the Pinnacle^3 treatment planning system as well as literature data of human anatomy approximation in Rando phantom in creation of the dose-volume histogram was also shown in this study.

As out-of-field doses are linked to an increase risk of development of SPC, it is advisable to provide radiation protective measures for the patient during high-energy external beam irradiation of the prostate to reduce the doses delivered to healthy distant organs. The use of Multileaf Shielding System (MSL) to protect

patient undergoing radiotherapy treatment with 18 MV medical linear accelerators from neutron exposure has been proposed previously (Rebello *et al* 2008). Other approaches which can reduce the doses delivered to healthy organs include the use of lower beam energy EBRT in order to minimize production of photoneutrons and/or provision of radiation protective shields to patient during treatment to reduce exposure to external secondary out-of-field radiations.

Chapter 8

Summary and conclusions

8.1 Summary of findings of this thesis and major conclusions

It is well recognized that radiotherapy given with the intent to cure any cancer including that of the prostate is associated with the risks of late normal tissue complications including the development of second primary cancers. The evaluation of radiation treatment plans is critical to ensure that the risks of late normal tissue complications are minimized without compromising the chances of cure of the cancer.

Dose-volume histograms (DVHs), one of the most frequently used and important parameters in the evaluation of the radiation treatment plans, provide the information about the physical distribution of radiation doses in and around the organs/tissues of interest. To enable the biological effects of different radiation treatment modalities and radiation dose schedules to be accounted for in the comparison of Normal Tissue Complication Probability (NTCP) and in the risk of Second Primary Cancer (SPC) the physical DVHs should be converted to Biologically Effective Dose ($BE_{ff}D$) and Equivalent Dose (D_{eq}) DVHs as has been done for the different radiation treatment modalities and dose fractionation schemes used at our centre.

The Relative Seriality and Lyman's NTCP models were applied to the $D_{eq}VHs$ of the organs-at-risk to derive the approximate "biological" NTCP of the organs-at-risk for a particular radiation treatment modality. The results suggest that brachytherapy either Low-Dose-Rate (LDR) or High-Dose-Rate (HDR) is associated with the lowest NTCP compared with any External Beam Radiotherapy (EBRT) technique for the treatment of the localized prostate cancer.

In the evaluation of risks of developing SPC, the competitive risk model was also applied to the $D_{eq}VHs$ to compare the different radiation techniques and dose schedules used. The rectum, bladder, and urethra represent the organs-at-risk because of their vicinity to the Planning Target Volume (PTV) around the prostate irradiated to prescribed (high) radiation dose. The competitive risk model was applied to the $D_{eq}VHs$ of these organs-at-risk and the effects of low and high radiation doses distributed in these organs-at-risk structures were taken into

account in the estimation of radiation-induced carcinogenesis. The average risk of developing SPC was no greater than 0.6% for all the treatment techniques and dose schedules used. Similar to NTCP, the risks of SPC associated with the brachytherapy treatment techniques were considerably lower than those of any of the EBRT techniques. In general, treatment plans which deliver equivalent doses of around 3 – 5 Gy to organs-at-risk have found to be associated with higher risks of developing SPC in the treatment technique and dose schedule used, due to the bell shape of the competitive risk model curve.

Evaluations of the $D_{eq}VHs$ of organs-at-risk for NTCP and the risks of SPC provide information of the radiobiological effects of radiation exposure in the vicinity of the prostate. However, during EBRT using high-energy (> 10 MeV) photon beams derived from medical linear accelerators, in addition to leakage photons, secondary neutrons, which have a higher radiobiological effect (RBE), are produced through the interactions of the high-energy photons with the components within the head of the linear accelerators. These secondary sources of radiations particularly neutrons raise concerns about the increased risk of induction of second malignancies in the organs/tissues outside of the radiation field of the prostate which received small but potentially significant radiation doses particularly with modern radiotherapy technique involving intensity modulation of the radiation beams.

The photon and neutron doses outside of the radiation field of the prostate were measured simultaneously using a novel radiation dosimetry technique based on ^{6}LiF:Mg,Cu,P and ^{7}LiF:Mg,Cu,P glass-rod TLDs located inside a Rando phantom. The technique of cross-calibration with the CR-39 etch-track detector was used to

derive the neutron readout-to-dose conversion factor for ^{6}LiF:Mg,Cu,P TLDs. The TLDs were placed in the approximate locations of the organs/tissues of interest inside the Rando phantom to measure the doses which resulted from the delivering of a dose of 80 Gy to the prostate using 4-field 3D-CRT technique using an 18 MV X-rays beam from Varian iX linear accelerator. The dose equivalents of the organs/tissues of interest are then estimated and the competitive risk model was applied to estimate the risk of SPC. The organs-at-risk such as thyroid, lungs, oesophagus, liver, spleen, and small and large intestines were exposed to different dose equivalents depending on the distance from the irradiation field and the estimated risks of SPC of these organs were ranged from 1.5% to 4.5%.

In conclusion, this study has shown that the contributions of high and low radiation doses resulting from various radiation treatment modalities and dose schedules used for the treatment of prostate cancer to NTCP and risk of SPC of organs-at-risk within and outside of the treatment volume can be relatively straightforwardly estimated using DVHs obtained from the planning systems. The findings have important implications for the development of optimal treatment techniques and dose schedules for the radiotherapeutic management of localized prostate cancer.

8.2 Future directions

Despite the wide range in radiosensitivity of organs-at-risk in patients with carcinoma of the prostate, the same radiation techniques and dose schedules are prescribed for patients with similar risk of relapse characteristics (Lee *et al* 2003). It has been shown here that NTCP and risks of SPC vary with the different

techniques and dose schedules. With the development of biomarkers which can reliably predict the radiosensitivity of individual patients, the radiation techniques and dose schedules which have the lowest NTCP and risk of SPC in the organs-at-risk as determined by the models in this thesis can be selected for radiosensitive individual if no other viable treatment such as surgery is available or appropriate.

The estimation of the risks of radiation-induced carcinogenesis following treatment of prostate cancer in this thesis does not take into account epidemiological factors which might modify these estimates such as smoking cigarettes for bladder carcinogenesis. The precision of these estimates can only be verified in prospective long term follow up studies of patients treated with the different radiation techniques and dose schedules to monitor the incidence of SPCs even though the risks are consistent with data based on population cohort studies. Pending verification of the precision of these model-based estimates, there is a need to incorporate these risk estimates into radiation treatment planning systems particularly with the impetus provided by on-line image guidance for the increasing implementation Intensity-Modulated Radiation Therapy (IMRT) for the treatment of localized carcinoma of the prostate.